Universal scaling between structural relaxation and vibrational dynamics in glass-forming liquids and polymers

L.Larini[⋆‡],A.Ottochian[⋆],C.De Michele[†·♯],D.Leporini[⋆♯]

[⋆]Dipartimento di Fisica "Enrico Fermi", Università di Pisa, Largo B. Pontecorvo 3, I-56127 Pisa, Italy

[†]Dipartimento di Fisica, Università di Roma "La Sapienza" Piazzale Aldo Moro, 2, 00185 Roma, Italy

[♯]INFM-CRS Soft, Piazzale Aldo Moro, 2, 00185 Roma, Italy

[‡] present address: Center for Biological Modeling and Simulation, University of Utah, Salt Lake City, Utah 84112-0850 USA

When liquids, polymers, bio-materials, metals and molten salts are cooled or compressed, if the crystallization is avoided, they freeze into a microscopically disordered solid-like state, a glass [1, 2]. On approaching the glass transition, the microscopic kinetic unit spends increasing time rattling with amplitude $< u^2 >^{1/2}$ on picosecond time scales within the cage of the first neighbours since the average escape time, the structural relaxation time τ_α, increases from a few picoseconds up to thousands of seconds. Despite the huge range of time scales older [3] and recent theoretical [4–9] studies addressed the underlying rattling process to understand the structural relaxation gaining support from numerical [10–13] and experimental works on liquids [14] and glasses [8, 15–19] with controversies [20] (for a review see

[21]). Here we show the universal correlation of the structural relaxation time (or the viscosity η) and the rattling amplitude from glassy to low-viscosity states by comparing computer simulations with experiments. According to the emerging picture the glass softens when the rattling amplitude exceeds a critical value in agreement with the Lindemann criterion for the melting of crystalline solids [22] and the free-volume model [23].

In the solid state of matter the atoms oscillate with mean square amplitude $< u^2 >$ around their equilibrium positions (henceforth to be referred to as the Debye-Waller factor, (DW)). With increasing temperature, solids meet different fates depending on the structural degree of order. In the crystalline state the ordered structure melts at T_m, whereas in the amorphous state the disordered structure softens at the glass transition temperature T_g above which flow occurs with viscosity η. The empirical law $T_g \simeq 2/3T_m$ [1, 2, 7] suggests that the two phenomena have a common basis. In fact, this viewpoint motivated extensions to glasses [24] of the Lindemann melting criterion for crystalline solids [22] and pictures the glass transition as a freezing in an aperiodic crystal structure (ACS) [5].

According to the ACS model, the viscous flow is due to activated jumps over energy barriers $\Delta E \propto k_B T a^2 / < u^2 >$ where a is the displacement to overcome the barrier, and k_B is the Boltzmann constant. The usual rate theory leads to the Hall-Wolynes equation (HW) $\tau_\alpha, \eta \propto \exp(a^2/2 < u^2 >)$ [5, 21]. $< u^2 >$ is the DW factor of the liquid, i.e. it is the amplitude of the rattling motion within

the cage of the surrounding atoms. That vibrational regime is assumed to occur on short time scales largely separated by the ones of the brownian diffusion. The ACS model is expected to fail when τ_α becomes comparable to the typical rattling times corresponding to picosecond timescales, a condition that is met at high temperatures (e.g. in selenium it occurs at $T_m + 104K$ [14]).

Several tests of the HW equation were carried out [21]. However, either the crystal or the glass contributions after extrapolation in the liquid regime are usually subtracted from $< u^2 >$. In selenium, the curve log η vs. $1/ < u^2 >$ is concave, whereas if the glass or the crystal contribution are removed, a convex curve or a straight line, the latter agreeing with the HW equation, are seen, respectively [14]. The fact that many glass-formers have no underlying crystalline phases, as well as the fact that in many studies removing the glass contribution, differently from selenium, leads to the HW equation, raises some ambiguities about the above subtractions.

It seems natural to generalize the HW equation by adopting a suitable distribution $p(a^2)$ of the square displacement to overcome the energy barriers, independent of state parameters, e.g. the temperature or the density. This is motivated by the observation that, irrespective of the relaxation time, the distance a particle moves during the structural relaxation is about the same, comparable to the molecular diameter [1]. Differently, the amplitude of the vibrational dynamics $< u^2 >$ is expected to be affected by state parameters [7, 9]. We choose a gaussian form for $p(a^2)$ with $\overline{a^2}$ average and $\sigma^2_{a^2}$ variance.

Averaging the HW equation over that distribution leads to:

$$\tau_\alpha, \eta \propto \exp\left(\frac{\overline{a^2}}{2 < u^2 >} + \frac{\sigma^2_{a^2}}{8 < u^2 >^2}\right). \quad (1)$$

Eq.1 yields the leading dependence on $< u^2 >$ even if the gaussian is truncated to account for a minimum displacement. In addition to the Central Limit Theorem, other motivations support the gaussian form of $p(a^2)$. For example, if the kinetic unit is undergoing a harmonic motion due to an effective spring with constant k, $< u^2 > \propto k_B T/k$, Eq.1 reduces to a form reported for both supercooled liquids [25] and polymers [26]. Furthermore, along the same line of reasoning, one may reinterpret the gaussian form of $p(a^2)$ as a gaussian distribution of the energy barriers $\Delta E \propto ka^2$ [27].

We show that the dependence of the structural relaxation time on the DW factor collapses to a universal master curve provided by Eq.1. We devised a two-step strategy. First, a master curve is constructed using extensive Molecular-Dynamics (MD) numerical simulations for a bead-spring model [28] of a polymer melt. Then a suitable scaling of both the numerical and experimental data is introduced to convert the MD master curve into the universal one including both strong and fragile glasses [1] and polymers; the latter, apart from a few studies [17, 19], were little considered.

We now discuss the MD simulations. They involved changes in the temperature T, the density ρ, the chain length M and the interaction potential $U_{p,q}(r)$. To characterize the short-time dynamics and the structural relaxation we use the monomer mean square displacement $< r^2(t) >$ (MSD) and the incoherent intermediate scattering function $F_s(q_{max}, t)$ (ISF), q_{max} being the q-vector of

the maximum of the static structure factor (see Methods).

Fig. 1 shows typical MSD and ISF curves. At very short times (ballistic regime) MSD increases according to $< r^2(t) > \cong (3k_BT/m)t^2$ and ISF starts to decay. The repeated collisions with the other monomers slow the displacement of the tagged one, evinced by a knee of MSD at $t \sim \sqrt{12}/\Omega_0 \sim 0.17$, where Ω_0 is an effective collision frequency: Ω_0 is the mean small-oscillation frequency of the monomer in the potential well produced by the surrounding ones kept at their equilibrium positions [29]. At later times a quasi-plateau region, also found in ISF, occurs when the temperature is lowered and/or the density increased. This signals the increased caging of the particle. The latter is released after an average time τ_α , defined by the relation $F_s(q_{max}, \tau_\alpha) = e^{-1}$ (other definitions differ by an overall constant due to the superposition of the ISF curves at long times by a suitable logarithmic shift, see inset of the lower panel of Fig. 1). For $t \gtrsim \tau_\alpha$ MSD increases more steeply. The monomers of short chains ($M \lesssim 3$) undergo diffusive motion $< r^2(t) > \propto t^\delta$ with $\delta = 1$. For longer chains, owing to the increased connectivity, the onset of the diffusion is preceded by a subdiffusive region ($\delta < 1$, Rouse regime) [23].

The dynamics of the model polymer depends in a complex way on the state parameters. Nonetheless, we systematically found that, if two states (labelled by multiplets $\{T, \rho, M, p, q\}$) have equal relaxation time τ_α, the corresponding MSD and ISF curves coincide from times fairly longer than τ_α down to the crossover to the ballistic regime and even at shorter times if the states have equal temperatures. Examples are shown in Fig.1. Notice that the coincidence

of MSD and ISF curves of states with equal τ_α at intermediate times ($t \lesssim \tau_\alpha$) must not be confused with the customary superposition of ISF curves at long times ($t \gtrsim \tau_\alpha$) following a suitable logaritmic time shift (see the lower-panel inset of Fig.1).

The above findings clearly shows that a correlation between the structural relaxation and the fast dynamics sets in. We assess it by correlating τ_α and the DW factor $< u^2 >$.

Preliminarily to the discussion of the DW factor we have to clarify whether the fast dynamics of the monomers takes place in cages. In this respect, we point out that the product $\Omega_0 \tau_\alpha \sim 20$ for states with the fastest relaxation and much larger for states with slower relaxation, i.e. the structure lifetime is at least one order of magnitude longer than the collision time. Furthermore, in the present study we always observe (not shown) that the time velocity correlation function (VCF), after a first large drop due to pair collisions, reverses the sign since the monomer rebounds from the cage wall [29].

We now show that the DW factor is a characteristic length scale of the rattling motion into the cage. The measure of the DW factor must take place in a time window where both the inertial and the relaxation effects are not present. To clearly identify that time window we consider the quantity $\Delta(t) \equiv \partial \log < r^2(t) > / \partial \log t$; representative plots of $\Delta(t)$ are given in the top inset of Fig.1. $\Delta(t)$ exhibits a clear minimum at $t^\star = 1.0(4)$ (corresponding to an inflection point in the log-log plot of $< r^2(t) >$) that separates two regimes. At short times, $t \lesssim 0.7 < t^\star$ VCF always exceeds the noise floor (not shown) and

the inertial effects become apparent. At long times ($t > \tau_\alpha > t^\star$) relaxation sets in. The short- and the long-time limits of $\Delta(t)$ correspond to the ballistic ($\Delta(0) = 2$) and the diffusive regimes ($\Delta(\infty) = 1$), respectively. To observe a minimum of $\Delta(t)$ requires that VCF exhibits a negative tail at long times. A monotonically decreasing VCF, i.e. no cage effect, leads to a monotonically decreasing $\Delta(t)$. Therefore, MSD at $t^\star$ is a mean localization length and the DW factor is $< u^2 > \equiv < r^2(t = t^\star) >$ (the same definition has been adopted, with no justification, in [11]). Notice that $t^\star$, corresponding to about $1 - 10ps$ [28], is consistent with the time scales of the experimental measurement of the DW factor, e.g. see [14].

Fig.2 shows the dependence of the structural relaxation time τ_α on DW factor. The data collapse on a well-defined master curve well fitted by Eq.1. States with different density, chain length and interaction potential are included in Fig.2 corresponding to different degrees of anharmonicity of the rattling motion into the cage (i.e. non-linear temperature dependence of the DW factor) and then to different fragilities [4, 7, 10, 12, 15, 18, 19, 21]. The scaling shows that for our model system both the average value $\overline{a^2}$ and the spread σ_{a^2} of the square displacement needed to overcome the energy barriers are not affected by the anharmonicity. The best-fit value of the average is $\overline{a^2}^{1/2} \cong 0.35$, consistent with both the observation that $< r^2(t = \tau_\alpha) >^{1/2} \lesssim 0.5$ (see Fig.1) and the well-known result that the atomic MSD during the structural relaxation is less than one atomic radius (~ 0.5 in MD units) [1].

The concavity of the master curve in Fig.2 is a signature of the heterogene-

ity of the structural relaxation. The best fit of our MD data with Eq.1 gives $\sigma_{a^2} \sim 0.25$ indicating a distribution of the displacement required to overcome the energy barriers. The magnitude of the ratio of the quadratic and the linear terms of Eq.1 with respect to $< u^2 >^{-1}$, $\mathcal{R} \equiv \sigma^2_{a^2}/4\overline{a^2} < u^2 >$, discriminates two different regimes. If the DW factor $< u^2 >$ is small enough that $\mathcal{R}$ is larger than one, the distribution of the displacement required to overcome the energy barriers shows up. In that case since different a values produce different monomer mobility, a heterogeneous mobility distribution is expected. On the other hand, if $\mathcal{R}$ is smaller than one, the dynamics is homogeneous. To support that scenario we recall that, on approaching the glass transition, a spatial distribution of mobilities develops with increasing non-gaussian features of the molecular displacement [2, 7, 30]. That features are characterized by the maximum $\alpha_{2\,max}$ of the time-dependent non-gaussian parameter $\alpha_2(t)$ (see Methods) [30]. The states with coinciding ISF and MSD shown in Fig.1 have coinciding $\alpha_2(t)$ curves too (not shown). For these states we sketch the relation between $\alpha_{2\,max}$ and $\mathcal{R}$ in the inset of Fig.2. It is seen that, when $\mathcal{R}$ exceeds the unit value, $\alpha_{2\,max}$ increases exponentially. Notably, the inset of Fig.2 reduces to an activated law for strong glassformers where $< u^2 >$ is nearly proportional to T; this law has been observed for silica [30].

Eq.1 with the best-fit parameters from Fig.2 offers the opportunity to find the DW factor $< u_g^2 >$ at the glass transition of the model polymer system. At the glass transition $\tau_\alpha = \tau_{\alpha\,g} \equiv 10^2 s$ in laboratory units [1] which corresponds to $\tau_{\alpha\,g} = 10^{13} - 10^{14}$ in dimensionless MD units (the time unit corresponds to

$1-10ps$ [28]). Eq.1 yields $< u_g^2 >^{1/2}= 0.129(1)$. This amplitude corresponds to the ratio $v_0 \sim (2 < u_g^2 >^{1/2})^3 = 0.017$ between the volume that is accessible to the monomer center-of-mass and the monomer volume. Flory and coworkers proposed that the glass transition takes place under iso-free volume conditions with the universal value $v_0 \cong 0.025$ [23]. Furthermore, an extension of the ACS model (leading to the HW equation) predicts that, just as for a crystalline solid [22] , there is a Lindemann criterion for the stability of glasses: the ratio $f =< u_g^2 >^{1/2} /d$, d being the average next neighbor distance of the atoms in the lattice, is a quasi-universal number ($f \cong 0.1$)[24]. Our data yield $f \sim 0.12-0.13$ (d is taken from the monomer radial distribution function) which is close to $f = 0.129$ for the melting of a hard sphere fcc solid [22].

We are now in a position to show that Eq.1 with the best-fit parameters from Fig.2 may be recast as a universal curve by considering the reduced variable $\tilde{x} =< u_g^2 > / < u^2 >$. For MD data we set $< u_g^2 >^{1/2}= 0.129$. Fig.3 shows scaling for several glassformers and polymers in a wide range of fragility. The scaling in Fig.3 must not be ascribed to $< u_g^2 >$ which does not correlate with the fragility m (compare m from Fig.3 and $< u_g^2 >$ from the Table in Supplementary Information). Instead, it shows that both the reduced mean square displacement $\overline{a^2}/ < u_g^2 >$ to overcome the energy barriers and the spread $\sigma_{a^2}/ < u_g^2 >$ are fragility-independent, and then also the curvature of the master curve which indicates the heterogeneity of the structural relaxation.

The experimental data in Fig. 3 were collected by changing the temperature. In this respect, the universal scaling of Fig.3 proves that the well-known

increasing deviation of $< u^2(T) >$ from the linear temperature dependence of the harmonic behavior by increasing the fragility index m [4, 7, 9, 18, 19] just mirrors the corresponding increasing bending of $\tau_\alpha(T)$ vs T_g/T in the Angell plot [1] from the glass transition region up to the liquid state. However, the glass transition may be reached under isothermal conditions by increasing the density or the connectivity (here expressed by the chain length) as well. Our MD results highlights the correlation of structural relaxation and vibrational dynamics also for these alternative routes. This prediction awaits experimental confirmation.

METHODS In our numerical simulations each chain is pictured as a freely-jointed linear sequence of M soft spheres, the monomers, with $M = 2, 3, 5, 10$. For details see Supplementary Information and ref.[28]. The non-bonded monomers belonging to the same or different chains interact via the potential $U_{p,q}(r) = \epsilon(q-p)^{-1}[p(\sigma^\star/r)^q - q(\sigma^\star/r)^p] + U_{cut}$ with $\sigma^\star = 2^{1/6}\sigma$ [12, 29]. All quantities are in reduced units: length in units of σ, temperature in units of ϵ/k_B, and time in units of $\sigma\sqrt{m/\epsilon}$, where m is the monomer mass. The potential is cut and shifted to zero by U_{cut} at $r = 2.5$. The bond length is $b = 0.97$. Changing the p and q parameters does not affect the position $r = \sigma^\star$ and the depth ϵ of the potential minimum but only the steepness of the repulsive and the attractive wings. The monomer mean square displacement (MSD) $< r^2(t) >$ is defined as: $< r^2(t) >= N^{-1} < \sum_{j=1}^{N} [\boldsymbol{r}_j(t) - \boldsymbol{r}_j(0)]^2 >$, where the sum runs over the total number of N monomers and the brackets denote a suitable ensemble average. The incoherent intermediate scattering function (ISF) $F_s(q_{max}, t)$ is defined as

$F_s(q,t) = N^{-1} < \sum_{j=1}^{N} exp\{-i\boldsymbol{q}\cdot[\boldsymbol{r}_j(t) - \boldsymbol{r}_j(0)]\} >$), q_{max} being the q-vector of the maximum of the static structure factor. The time-dependent non-gaussian parameter is defined as $\alpha_2(t) = \frac{3<r^4(t)>}{5<r^2(t)>^2} - 1$ and vanishes if the displacement r is gaussian.

To prepare Fig.3, data about the structural relaxation (in seconds) and the viscosity (in Pa·s) were scaled to the MD master curve by logarithmic vertical shifts +11.5(5) and +1.5(5), respectively, apart from B_2O_3 (+8.4(5) and −2.2(5)). Data of polymers refer to τ_α. Data related to B_2O_3, OTP, Ferrocene/Dibutylphthalate include two independent sets, one for τ_α, the other for η, which for simplicity's sake are presented with the same symbol. See Supplementary Information for the data sources and further details.

References

[1] Angell, C.A. Relaxation in liquids, polymers and plastic crystals - strong/fragile patterns and problems. *J.Non-Crystalline Sol.* **131-133**, 13-31 (1991).

[2] Debenedetti, P. G. & Stillinger, F. H. Supercooled liquids and the glass transition. *Nature* **410**, 259-267 (2001).

[3] Tobolsky, A., Powell, R. E. & Eyring, H. in *Frontiers in Chemistry* (eds Burk, R. E. & Grummit, O.) Vol. 1, 125-190 (Interscience, New York , 1943).

[4] Angell, C. A. Formation of glasses from liquids and biopolymers. *Science* **267**, 1924-1935 (1995).

[5] Hall, R. W. & Wolynes, P. G. The aperiodic crystal picture and free energy barriers in glasses. *J. Chem. Phys.* **86**, 2943-2948 (1987).

[6] Dyre, J. C., Olsen, N. B. & Christensen, T. Local elastic expansion model for viscous-flow activation energies of glass-forming molecular liquids. *Phys. Rev. B* **53**, 2171-2174 (1996).

[7] Ngai, K.L. Dynamic and thermodynamic properties of glass-forming substances. *J. Non-Cryst. Solids* **275**, 7-51 (2000).

[8] Martinez, L.-M. & Angell, C. A. A thermodynamic connection to the fragility of glass-forming liquids. *Nature* **410**, 663-667 (2001).

[9] Ngai, K.L. Why the fast relaxation in the picosecond to nanosecond time range can sense the glass transition. *Phil. Mag.* **84**, 1341-1353 (2004).

[10] Shao, J. & Angell, C.A. Vibrational anharmonicity and the glass transition in strong and fragile vitreous polymorphs. *Proc. XVIIth International Congress on Glass, Beijing*, **1**, 311-320 (1995)

[11] Starr, F. W., Sastry, S., Douglas, J. F. & Glotzer, S. What do we learn from the local geometry of glass-forming liquids? *Phys. Rev. Lett.* **89**, 125501 (2002).

[12] Bordat, P., Affouard, F., Descamps, M. & Ngai, K.L. Does the interac-

tion potential determine both the fragility of a liquid and the vibrational properties of its glassy state? *Phys. Rev. Lett.* **93**, 105502 (2004).

[13] Widmer-Cooper, A. & Harrowell, P. Predicting the Long-Time Dynamic Heterogeneity in a Supercooled Liquid on the Basis of Short-Time Heterogeneities. *Phys. Rev. Lett.* **96**, 185701(4) (2006).

[14] Buchenau, U. & Zorn, R. A relation between fast and slow motions in glassy and liquid selenium. *Europhys. Lett.* **18**, 523-528 (1992).

[15] Sokolov, A. P., Rössler, E., Kisliuk, A. & Quitmann, D. Dynamics of strong and fragile glass formers: Differences and correlation with low-temperature properties. *Phys. Rev. Lett.* **71**, 2062-2065 (1993).

[16] Scopigno, T., Ruocco, G., Sette, F. & Monaco, G. Is the fragility of a liquid embedded in the properties of its glass? *Science* **302**, 849-852 (2003).

[17] Buchenau, U. & Wischnewski, A. Fragility and compressibility at the glass transition. *Phys. Rev. B* **70**, 092201 (2004).

[18] Novikov, V. N. & Sokolov, A. P. Poisson's ratio and the fragility of glass-forming liquids. *Nature* **431**, 961-963 (2004).

[19] Novikov, V. N., Ding,Y. & Sokolov, A. P. Correlation of fragility of supercooled liquids with elastic properties of glasses. *Phys.Rev.E* **71**, 061501(2005).

[20] Yannopoulos, S. N. & Johari, G. P. Poisson's ratio and liquid's fragility. *Nature* **442**, E7-E8 (2006).

[21] Dyre, J. C. The glass transition and elastic models of glass-forming liquids. *Rev.Mod.Phys.* **78**, 953-972 (2006).

[22] Löwen, H. Melting, freezing and colloidal suspensions. *Phys. Rep.* **237**, 249-324 (1994).

[23] Gedde, U.W. *Polymer Physics* (Chapman and Hall, London, 1995).

[24] Xia, X. & Wolynes, P.G. Fragilities of liquids predicted from the random first order transition theory of glasses. *PNAS* **97**, 2990-2994 (2000).

[25] Bässler, H. Viscous flow in supercooled liquids analyzed in terms of transport theory for random media with energetic disorder. *Phys. Rev. Lett.* **58**, 767-770 (1987).

[26] Ferry, J.D., Grandine, L. D. Jr. & Fitzgerald, E. R. The relaxation distribution function of polyisobutylene in the transition from rubber-like to glass-like behavior. *J. Appl. Phys.* **24**, 911-916 (1953).

[27] Monthus, C. & Bouchaud, J.-P. Models of traps and glass phenomenology. *J. Phys. A: Math. Gen.* **29**, 3847-3869 (1996).

[28] Kröger, M. Simple models for complex nonequilibrium fluids. *Phys. Rep.* **390**, 453-551 (2004).

[29] Boon, J. P. & Yip, S. *Molecular Hydrodynamics* (Dover Publications, New York, 1980).

[30] Glotzer S.C. & Vogel M. Temperature dependence of spatially heterogeneous dynamics in a model of viscous silica. *Phys. Rev. E* **70,**, 061504 (2004).

Supplementary Information: Supplementary information accompanies this paper.

Competing interests statement: The authors declare no competing financial interests.

Correspondence and requests for materials should be addressed to D.L. (e-mail: dino.leporini@df.unipi.it).

Acknowledgements The authors acknowledge discussions with C.A.Angell, S.Capaccioli, G.Carini, P.G.Debenedetti, J.Dyre, A.Fontana, K.L.Ngai, G.Ruocco, F.Sciortino, S.N.Shore. A. Wischnewski is thanked for providing the DW data of silica. Computational resources by "Laboratorio per il Calcolo Scientifico" (Physics Department, University of Pisa) and financial support from MIUR within the PRIN project "Aging, fluctuation and response in out-of-equilibrium glassy systems" are acknowledged.

Figure 1: **MD simulations of the polymer melt**. Top: MSD time-dependence in selected cases (see Supplementary Information). MSDs are multiplied by indicated factors. Inset: corresponding MSD slope $\Delta(t)$; the uncertainty range on the position of the minimum at $t^\star = 1.0(4)$ (black line) is bounded by the vertical colored lines. Bottom: corresponding ISF curves. Inset: superposition of the ISF curves. Four sets of clustered curves (A through D) show that, if states have equal τ_α (marked with dots on each curve), the MSD and ISF curves coincide from times fairly longer than τ_α down to the crossover to the ballistic regime at least.

Figure 2: **The structural relaxation time τ_α vs the DW factor $< u^2 >$ from MD simulations**. Circles identify the cases plotted in Fig.1. The dashed curve is Eq. 1 $\log \tau_\alpha = \alpha + \beta < u^2 >^{-1} + \gamma < u^2 >^{-2}$ with $\alpha = -0.424(1), \beta = \overline{a^2}/2 \ln 10 = 2.7(1) \cdot 10^{-2}, \gamma = \sigma^2_{a^2}/8 \ln 10 = 3.41(3) \cdot 10^{-3}$. Additional data on the collective relaxation time τ are also plotted ($\triangledown$) [11]. The dotted curve is obtained by vertically shifting the dashed curve ($\alpha' = \alpha + 0.205(5)$). Inset: the maximum of the non-gaussian parameter $\alpha_{2\ max}$ of the A-E clusters of states vs. the ratio of the quadratic and the linear terms of Eq.1 with respect to $< u^2 >^{-1}$.

Figure 3: **Scaling of the structural relaxation time τ_α (in MD units) vs. the reduced mean square amplitude** $\tilde{x} =< u_g^2 > / < u^2 >$. The grey area marks the glass transition. The continuous black line is Eq.1 rewritten as $\log \tau_\alpha = \alpha + \tilde{\beta}\tilde{x} + \tilde{\gamma}\tilde{x}^2$ with $\tilde{\beta} = \beta/0.129$ and $\tilde{\gamma} = \gamma/0.129^2$; α, β, γ from Fig.2. The numbers in parenthesis denote the fragility m. The uncertainty on the time $t^\star = 1 \pm 0.4$ involved in the definition of the DW factor ($< u^2 > \equiv < r^2(t = t^\star) >$) leads to an error on the black curve which is bounded between the two colored continuous curves corresponding to the two definitions $< u^2 > \equiv < r^2(t = 0.6) >$ (magenta, $< u_g^2 >^{1/2} = 0.134(1)$) and $< u^2 > \equiv < r^2(t = 1.4) >$ (orange, $< u_g^2 >^{1/2} = 0.122(1)$).

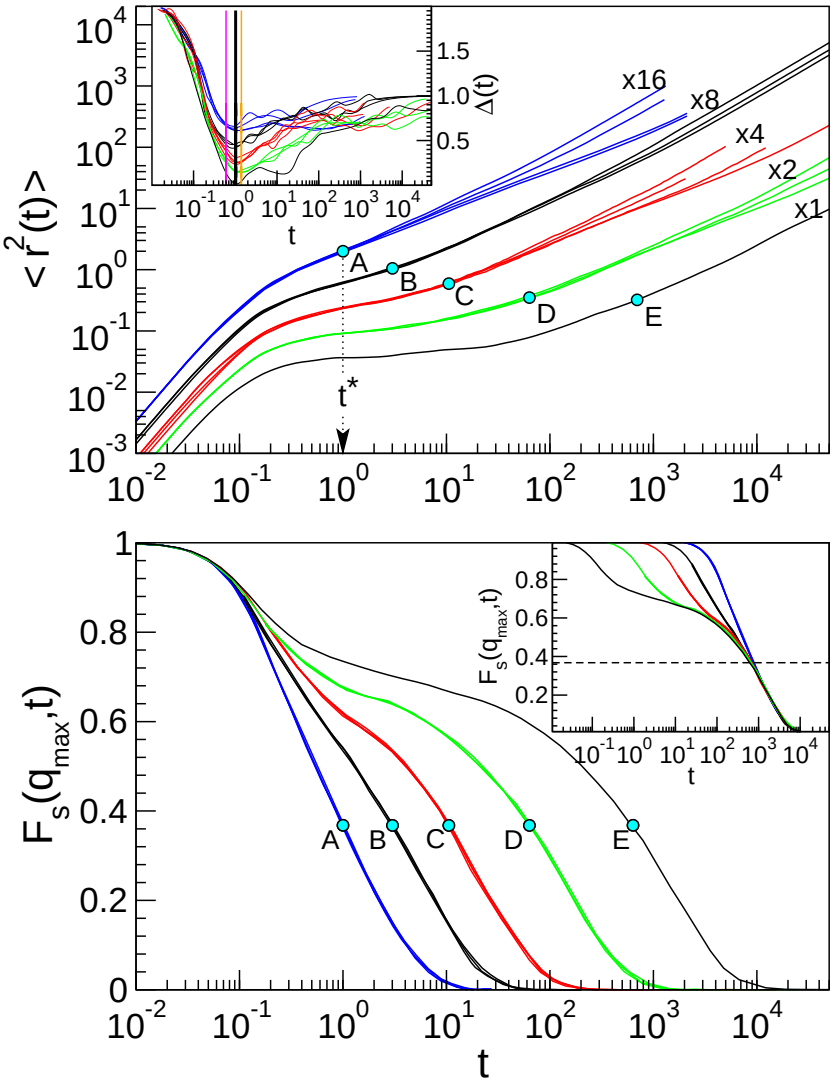

FIGURE 1

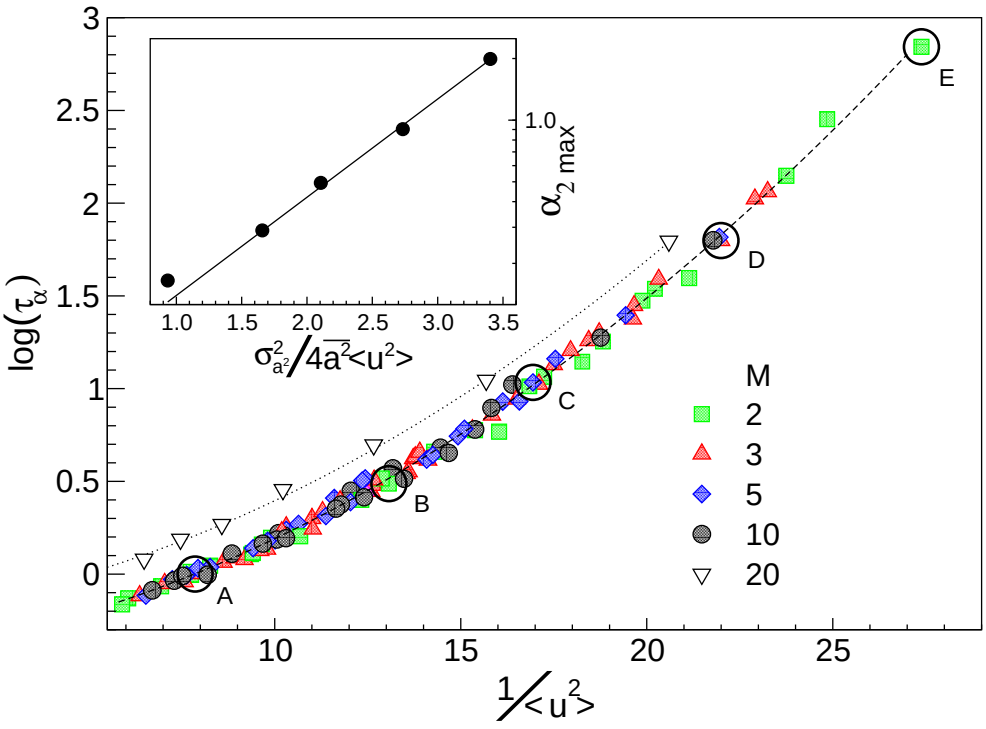
log(τα)
1/<u2>
A
B
C
D
E
M
2
3
5
10
20
α2 max
σ2a2/4a2<u2>
1.0
1.5
2.0
2.5
3.0
3.5
0
0.5
1
1.5
2
2.5
3
10
15
20
25

FIGURE 2

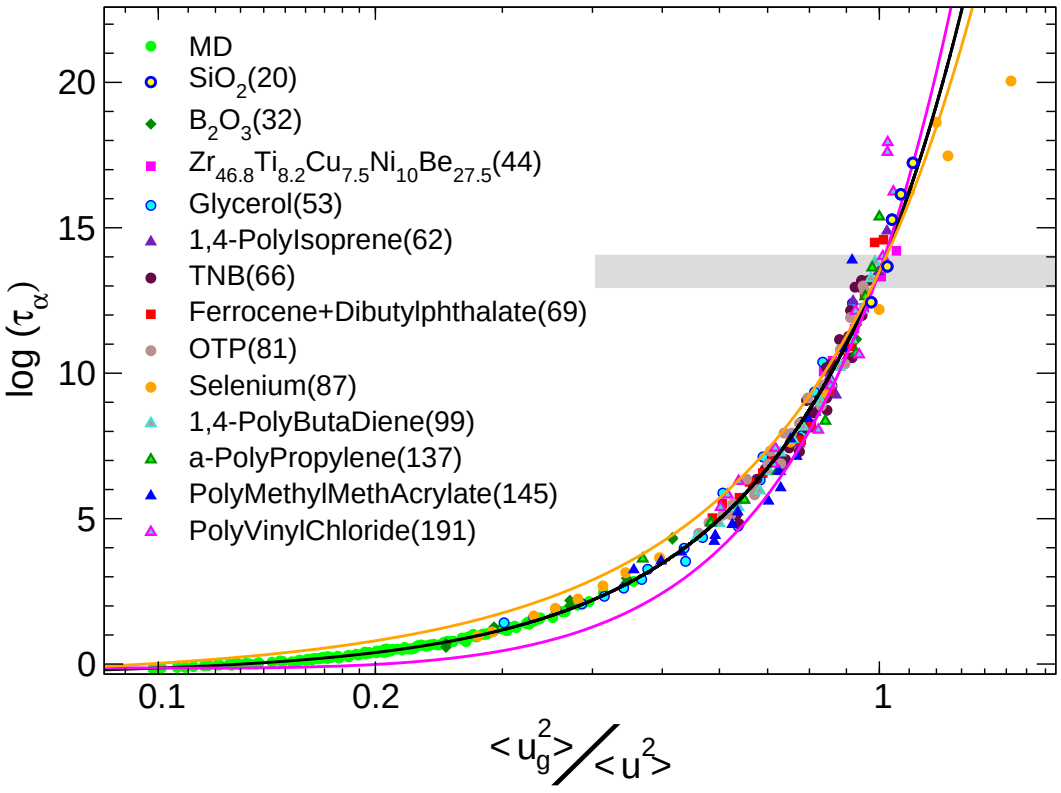
MD
SiO2(20)
B2O3(32)
Zr46.8Ti8.2Cu7.5Ni10Be27.5(44)
Glycerol(53)
1,4-PolyIsoprene(62)
TNB(66)
Ferrocene+Dibutylphthalate(69)
OTP(81)
Selenium(87)
1,4-PolyButaDiene(99)
a-PolyPropylene(137)
PolyMethylMethAcrylate(145)
PolyVinylChloride(191)
log (τα)
0
5
10
15
20
0.1
0.2
1
<ug2>/<u2>

FIGURE 3

1 Simulations

In this section the model of the polymer melt and the numerical techniques being used in the simulations are briefly summarized.

1.1 Force field

A coarse-grained model of a linear polymer chain is used. Torsional potentials are neglected. Each monomer is pictured as a soft sphere interacting via a suitable pair potential with the other non-bonded monomers. Bonded monomers interact with a potential which is the sum of the FENE (Finitely Extendible Nonlinear Elastic) potential and the Lennard-Jones potential [1]:

$$U_{\mathrm{LJ}}(r) = \epsilon \left[\left(\frac{\sigma^*}{r} \right)^{12} - 2 \left(\frac{\sigma^*}{r} \right)^{6} \right] \tag{1}$$

$$U_{\mathrm{FENE}}(r) = -\frac{1}{2} k R_0^2 \ln \left[1 - \left(\frac{r}{R_0} \right)^2 \right], \quad R_0 = 1.5\sigma, \quad k = \frac{30\epsilon}{\sigma^2} \tag{2}$$

where r is the monomer-monomer distance and $\sigma^* = 2^{1/6}\sigma$. With the above parameters the bond length is $b = 0.97\sigma$ within few percent.

Non-bonded monomers interact via a truncated parametric Lennard-Jones potential [1]:

$$U_{p,q}(r) = \begin{cases} \dfrac{\epsilon}{q-p} \left[p \left(\dfrac{\sigma^*}{r} \right)^q - q \left(\dfrac{\sigma^*}{r} \right)^p \right] + U_{cut} & r \leqslant r_c \\ 0 & \text{Otherwise} \end{cases} \tag{3}$$

where the value of the constant U_{cut} is chosen to ensure $U_{p,q}(r_c) = 0$ at $r = r_c = 2.5\sigma$. The minimum of the potential $U_{p,q}(r)$ is at $r = \sigma^*$, with a constant depth $U(r = \sigma^*) = \epsilon$. We set $\sigma = 1, \epsilon = 1$. The time unit is $\tau_{MD} = (m\sigma^2/\epsilon)^{1/2}$, with m being the mass of the monomer. Temperature is in units of ϵ/k_B, where k_B is the Boltzmann constant. We set $m = k_B = 1$.

1.2 Statistical ensembles

The simulations were performed using three distinct ensembles: isothermal-isobaric ensemble (NPT), canonical ensemble (NTV) and microcanonical en-

semble (NVE). NPT and NTV ensembles have been used for equilibration runs while NVE ensemble has been used for production runs.

1.3 Algorithm

NPT and NTV ensembles have been simulated with the extended system method introduced by Andersen [2] and Nosé [3]. Within this approach, additional degrees of freedom are added to the Hamiltonian of the system, to be interpreted as the degrees of freedom associated to the thermal piston and the mechanical one. The numerical integration of the augmented Hamiltonian has been performed through the reversible multiple time steps algorithm (i.e. the r-RESPA algorithm) developed by Tuckerman *et al.*[4]. In particular, the NPT and NTV Liouville operators corresponding to the aforementioned extended Hamiltonian have been factorized using the Trotter theorem [5] separating the short range and long range contributions of the potential $U_{p,q}(r)$, Eq. 3, according to the WCA decomposition [6]. The simulations have a drift of the total energy less than $\sim 5 \cdot 10^{-8}\epsilon/\tau_{MD}$ and a standard deviation of the total energy less than $2 \cdot 10^{-4}$ with an integration time step $3 \cdot 10^{-3}\tau_{MD}$. The latter was kept constant in all the production runs to limit systematic errors. To speed-up the simulations, we exploited the neighbour lists method and, to reduce the finite-size effects, periodic boundary conditions have been used.

1.4 Simulation protocol

In this section the simulation protocol is described. Each state point (labelled by the multiplets $\{T, \rho, M, p, q\}$) has been obtained through four stages:

1. Placement of the chains in a regular lattice preventing monomer-monomer overlap.

2. NPT-ensemble simulation to get the number density of interest ρ.

3. NTV-ensemble equilibration of the system. The equilibration time is ten times longer than the longest relaxation time, i.e. the time needed by the end-to-end correlation function to decay to less than 0.1 times its initial value.

4. NVE-ensemble production run.

1.5 Data set

We investigated 121 indipendent states. Both the temperature T, the number density ρ, the monomers per chain M and the parameters p, q in the force field, eq. 3, are changed. $\rho = N/V$ where N is the total number of monomers, and V is the volume of the cubic box. $N = 2000$ in all cases but $M = 3$ where $N = 2001$. For each case averages on at least five indipendent configurations are performed. For $M = 10$ the least number of indipendent configurations is ten. Below, the different state points are listed. In addition to the sistematic scan of some parameters, other cases were added to ensure the optimum definition of the master curve plotted in Fig.2.

$T = 0.7$:

- $p = 6$. All the combinations with $M = 2, 3, 5, 10$, $\rho = 1.033, 1.056, 1.086$ and $q = 7, 8, 10, 12$. The case $M = 2, \rho = 1.086, q = 12$ equilibrates very slowly and was discarded.
- $p = 6, M = 3$. The pairs (ρ, q): (1.090,12), (1.033,11), (1.039,11), (1.041,11), (1.045,11), (1.051,11), (1.056,11), (1.086,11), (1.033,9), (1.056,9), (1.063,9), (1.071,9), (1.079,9), (1.086,9).
- $p = 5, q = 8$. All the combinations with $M = 2, 3, 5, 10$ and $\rho = 1.133, 1.156, 1.186, 1.2$. Furthermore, $M = 2$, $\rho = 1.033$.
- $p = 11, q = 12, M = 2$ with densities $\rho = 0.980, 0.990, 1.0$.

$T \neq 0.7, p = 6$:

- $T = 0.5$, $\rho = 1.033$, All the combinations with: $M = 2, 3, 5, 10$, $q = 7, 8, 10$.
- $T = 0.6$, $\rho = 1.033$, All the combinations with: $M = 2, 3, 5, 10$, $q = 8, 10$.
- $q = 12$, $\rho = 1.033$, the pairs (M, T): (2,0.5), (3,0.5), (2,0.55), (3,0.55), (2,0.6), (3,0.6), (5,0.6), (3,0.65), (5,0.65), (10,0.65).
- $q = 12$, $\rho = 1.086$, the pairs (M, T): (2,0.75), (3,0.75), (5,0.75), (10,0.75), (2,0.8), (3,0.8), (5,0.8).
- $q = 12, \rho = 1.090, M = 3$, with $T = 0.75, 0.8$.

Finally, $p = 5, q = 8, M = 2, \rho = 1.033, T = 0.5$.

1.6 Data sets of Fig. 1

The data sets of Fig. 1 are the multiplets (M, ρ, T, q, p):

- Set A (blue): (2,1.086,0.7,7,6), (3,1.086,0.7,7,6), (10,1.086,0.7,7,6), (10,1.033,0.7,8,6)
- Set B (black): (2,1.033,0.7,10,6), (3,1.039,0.7,11,6), (3,1.041,0.7,11,6)
- Set C (red): (2,1.033,0.5,10,6), (3,1.056,0.7,12,6), (5,1.033,0.6,12,6), (10,1.056,0.7,12,6)
- Set D (green): (3,1.086,0.7,12,6), (5,1.086,0.7,12,6), (10,1.086,0.7,12,6)
- Set E:(2,1.0,0.7,12,11)

2 Experimental data and scaling

The Section gives information on the sources of the experimental data and the scaling procedure leading to Fig. 3. We adopted the customary definition of the glass transition temperature T_g, i.e. the temperature where the structural relaxation time $\tau_\alpha = 100\ s$ or the viscosity $\eta = 10^{12}\ Pa \cdot s$.

2.1 Data sources

For each system the temperature dependencies of the mean square displacement $< u^2 >$ and τ_α or η are used. The pairs $(< u^2 >, \tau_\alpha)$ or $(< u^2 >, \eta)$ are preferably taken from the same source, if possible. In the absence of a single paper, the pairs are taken from different sources provided that the temperature ranges of the two studies overlap meaningfully and include the glass transition region. For some systems both viscosity and structural relaxation data were considered. The mean square displacements $< u^2 >$ are drawn from incoherent neutron scattering (INS) and Mössbauer spectroscopy (MS). The former takes $< u^2 >$ from the Debye-Waller Factor, the latter from the Lamb-Mössbauer factor $f \propto \exp(-q^2 < u^2 >)$ with $q = 7.3\text{Å}^{-1}$. The fragilities were drawn from refs. [7, 8]. The structural relaxation (in seconds) and the viscosity (in Pa·s) were scaled to the MD master curve by logarithmic vertical shifts in Fig. 3. Table 1 lists in order of increasing fragility the systems, the data sources for τ_α or η, the vertical shifts, the

Table 1: Relevant information about the investigated systems (in order of increasing fragility) and the MD simulations. The structural relaxation time is taken via either dielectric spectroscopy or, for a part of the data set of B_2O_3, data aggregated from different techniques. The mean square displacement is taken from Incoherent Neutron Scattering (INS) or Mössbauer Spectroscopy (MS). The logarithmic vertical shifts to scale the experimental curves to the MD master curve in Fig. 3 and the mean square displacement at T_g, $< u_g^2 >$ in Å^2 (or $-\ln f_g$ for MS), are also given.

system	$\tau_\alpha,\ \eta$			$< u^2 >$		
	quantity	shift	ref.	technique	$< u_g^2 >$ $-\ln f_g$	ref.
MD	MD	0		MD	0.01667	
SiO_2	η	+2	[9]	INS	0.081	[10]
B_2O_3	η	-2.2	[11]	INS	0.065	[12]
B_2O_3	$\tau_\alpha^\dagger$	+8.4	[13]	INS	0.065	[12]
$Zr_{46.8}Ti_{8.2}Cu_{7.5}Ni_{10}Be_{27.5}$	η	+1	[14]	MS	0.885	[15]
Glycerol	η	+1	[16]	INS	0.022	[17]
PI	τ_α	+12	[18]	INS	0.427	[19]
TNB	η	+2	[20]	INS	0.315	[21]
Fe+DBP	τ_α	+11	[22]	MS	3.15	[22]
Fe+DBP	η	+2	[23]	MS	3.05	[22]
OTP	τ_α	+11	[21]	INS	0.215	[24]
OTP	η	+1	[24]	INS	0.232	[24]
Selenium	η	+1.66	[25]	INS	0.155	[25]
1,4 PBD	τ_α	+11	[26]	INS	0.102	[27, 28]
a-PP	τ_α	+11.5	[29]	INS	0.13	[30]
PMMA	τ_α	+11.5	[31]	INS	1.1	[32]
PVC	τ_α	+11	[33]	INS	0.51	[32]

† data aggregated from different techniques.

experimental technique used to measure $< u^2 >$ and its value at T_g, $< u_g^2 >$ (or $-\ln f_g$ for Mössbauer experiments).

Notice that for B_2O_3 two independent sets concerning τ_α and η were considered. The shifts of τ_α and η of B_2O_3 differ about three orders of magnitude with respect to the ones of the other systems. However, the difference between the shifts of the two sets ($+10.6$) is close to the difference of the shifts of the other systems ($\simeq +10.0(7)$).

References

[1] Baschnagel, J. & Varnik, F. Computer simulations of supercooled polymer melts in the bulk and in confined geometry. *J. Phys.: Condens. Matter* **17**, R851-R953 (2005).

[2] Andersen, H. C. Molecular dynamics simulations at constant pressure and/or temperature. *J. Chem. Phys.* **72**, 2384-2393 (1980).

[3] Nosé, S. A unified formulation of the constant temperature molecular dynamics methods. *J. Chem. Phys.* **81**, 511-519 (1984).

[4] Tuckerman, M. E., Berne, B. J. & Martyna, G. J. Reversible multiple time scale molecular dynamics. *J. Chem. Phys.* **97**, 1990-2001 (1992).

[5] Trotter, H. F. On the Product of Semi-Groups of Operators. *Proc. Am. Math. Soc.* **10**, 545-551 (1959).

[6] Tuckerman, M. E., Berne, B. J. & Martyna, G. J. Molecular dynamics algorithm for multiple time scales: Systems with long range forces. *J. Chem. Phys.* **94**, 6811-6815 (1991).

[7] Böhmer, R., Ngai, K. L., Angell, C. A. & Plazek, D. J. Nonexponential relaxations in strong and fragile glass formers. *J. Chem. Phys.* **99**, 4201-4209 (1993).

[8] Qin, Q. & McKenna, G. B. Correlation between dynamic fragility and glass transition temperature for different classes of glass forming liquids. *J. Non-Cryst. Solids* **352**, 2977-2985 (2006).

[9] Doremus, R. H. Viscosity of silica *J. Appl. Phys.* **92**, 7619-7629 (2002).

[10] Wischnewski A. , *Ph.D. Thesis* (Heinrich-Heine Universität , Düsseldorf, 1998).

[11] Bernatz, K. M., Echeverría, I., Simon, S. L. & Plazek, D. J. Viscoelastic properties of boron dioxide. *J. Non-Cryst. Solids* **289**, 9-16 (2001).

[12] Engberg, D., Wischnewski, A., Buchenau, U., Börjesson, L., Dianoux, A. J., Sokolov, A. P. & Torell, L. M. Sound waves and other modes in the strong glass former B_2O_3. *Phys. Rev. B* **58**, 9087-9097 (1998).

[13] Sidebottom, D., Bergman, R., Börjesson, L. & Torell, L. M. Two-step relaxation decay in a strong glass former. *Phys. Rev. Lett.* **71**, 2260-2263 (1993).

[14] Busch, R., Bakke, E. & Johnson, W. L. Viscosity of the supercooled liquid and relaxation at the glass transition of the $Zr_{46.8}Ti_{8.2}Cu_{7.5}Ni_{10}Be_{27.5}$ bulk metallic glass forming alloy *Acta Mater.* **46**, 4725-4732 (1998).

[15] Meyer, A., Franz, H., Sepiol, B., Wuttke, J. & Petry, W. Fast relaxation in a metastable metallic melt. *Europhys. Lett.* **36**, 379-384 (1996).

[16] Cummins, H. Z., Hernandez, J., Du, W. M. & Li, G. Comment on "Anomalies in the Scaling of the Dielectric α-Relaxation". *Phys. Rev. Lett.* **73**, 2935-2935 (1994).

[17] Wuttke, J., Petry, W., Coddens, G. & Fujara, F.; Fast dynamics of glass-forming glycerol. *Phys. Rev. E* **52**, 4026-4034 (1995).

[18] Roland, C. M., Schroeder, M. J., Fontanella, J. J. & Ngai, K. L. Evolution of the Dynamics in 1,4-Polyisoprene from a Nearly Constant Loss to a Johari-Goldstein β-Relaxation to the α-Relaxation. *Macromolecules* **37**, 2630-2635 (2004).

[19] Frick, B. & Fetters, L. J. Methyl Group Dynamics in Glassy Polyisoprene: A Neutron Backscattering Investigation. *Macromolecules* **27**, 974-980 (1994).

[20] Plazek, D. J. & Magill, J. H. Physical Properties of Aromatic Hydrocarbons. IV. An Analysis of the Temperature Dependence of the Viscosity and the Compliance of 1,3,5 Tri-α-naphthylbenzene. *J. Chem. Phys.* **49**, 3678-3682 (1968).

[21] Ngai, K. L. Dynamic and thermodynamic properties of glass-forming substances. *J. Non-Cryst Solids* **275**, 7-51 (2000).

[22] Franz, H., Petry, W. & Baron, A.Q.R. Quasielastic scattering: slow dynamics of glasses. *Hyperfine Interact.* **123/124**, 865-879 (1999).

[23] Menon, N., Nagel, S. R. & Venerus, D. C. Dynamic Viscosity of a Simple Glass-Forming Liquid. *Phys. Rev. Lett.* **73**, 963-966 (1994).

[24] Tölle A. Neutron scattering studies of the model glass former *ortho*-terphenyl. *Rep. Prog. Phys.* **64**, 1473-1532 (2001).

[25] Buchenau, U. & Zorn R. A relation between fast and slow motions in glassy and liquid selenium. *Europhys. Lett.* **18**, 523-528 (1992).

[26] Zorn R. Microscopic dynamics of glass-forming polymers. *J. Phys.: Condens. Matter* **15**, R1025-R1046 (2003).

[27] Frick, B. & Richter, D. The microscopic basis of the glass transition in polymers from neutron scattering studies. *Science* 267, 1939-1945 (1995).

[28] Frick, B., Richter, D., Petry, W. & Buchenau U. Study of the glass transition order parameter in amorphous polybutadiene by incoherent neutron scattering. *Z. Phys. B* **70**, 73-79 (1988).

[29] Roland, C. M., Ngai, K. L., Santangelo, P. G., Qiu, X. H., Ediger, M. D. & Plazek, D. J. Temperature Dependence of Segmental and Terminal Relaxation in Atactic Polypropylene Melts. *Macromolecules* **34**, 6159-6160 (2001).

[30] Kanaya, T., Kaji, K., Bartos, J. & Klimova, M. Onset of the Fast Process in Amorphous Polypropylene as Detected by Quasielastic Neutron-Scattering and Electron Spin Resonance Techniques. *Macromolecules* **30**, 1107-1110 (1997).

[31] Colby, R. H. Dynamic scaling approach to glass formation. *Phys. Rev. E* **61**, 1783-1792 (2000).

[32] Soles, C. L., Douglas, J. F., Wu, W.-I. & Dimeo, R.M. Incoherent Neutron Scattering as a Probe of the Dynamics in Molecularly Thin Polymer Films. *Macromolecules* **36**, 373-379 (2003).

[33] McCrum, N.G., Read, B.E. & Williams, G. *Anelastic and Dielectric Effects in Polymeric Solids*(Dover Publications, New York, 1991).